JOURNAL OF GEOPHYSICAL RESEARCH, VOL. 106, NO. C4, PAGES 6917-6929, APRIL 15, 2001

Summer transport through the Tsushima-Korea Strait

G.A. Jacobs, H. T. Perkins, W. J. Teague, and P. J. Hogan

Naval Research Laboratory, Stennis Space Center, Mississippi

Abstract. Transport variations through the Korea-Tsushima Strait are examined from two lines of bottom-moored acoustic doppler current profilers (ADCPs) deployed southwest and northeast of Tsushima Island in May 1999. Almost full-depth velocity profiles are measured. An optimal interpolation (OI) scheme is used to interpolate the data spatially and to provide error estimates along each section. The strong northeastward current core through the southern section lies approximately in the center of the strait, and small southwestward flows occur sporadically near both the Korea and Japan coasts. Much of the flow through the northern line occurs near the Korea and Japan coasts, with a weak southwestward mean flow and large variability in the strait center on the leeside of Tsushima Island. The estimated mean transport is 2.9 sverdrups (Sv) through the southern line and 2.5 Sv through the northern line. The northern line does not extend close to the Korea coast where there is significant flow. Expected errors in the transport estimates at any time are about 0.5 Sv RMS for each mooring line. The gradual transport increase through the summer is carried through the center of the southern line and on the Korea side of the strait through the northern line.

1. Introduction

Transport through the Korea-Tsushima Strait (hereafter referred to as the strait) contains short spatial scales (<50 km) as well as short temporal scales (<20 days). Several approaches have been used to estimate total transport as well as transport variability through the strait. Some of the earliest transport variability estimates are based on variations in the sea level drop across the strait and the assumption that the flow is geostrophic, with the Coriolis force balancing the cross-strait pressure gradient. In addition, it is assumed that the currents are mainly barotropic. *Yi* [1966] uses sea level variations measured at tide gauge stations at Pusan, Cheju, and Izuhara to deduce a mean current of 48.5 cm/s with an annual variability of 38.5 cm/s (peak to peak). *Katoh* [1993] uses shipboard ADCP measurements with simultaneous temperature and salinity measurements to demonstrate that the flow is roughly in geostrophic balance. The assumption that the flow is barotropic is not entirely accurate. Thus *Isobe* [1994] combines sea level observations on opposite sides of the strait to determine barotropic transport and uses hydrographic observations to account for baroclinic compensation effects. The seasonal transport variability of 0.7 Sv is observed through this method.

Shipboard acoustic doppler current profiler (ADCP) measurements also have provided a useful tool for measuring the strait transport. *Isobe et al.* [1994] examine five ADCP surveys utilizing a ship-towed instrument along a section from Korea to Japan northeast of Tsushima Island during 1990 - 1991. A maximum transport of 5.6 Sv is observed in September and about 1.2 Sv at other times. *Katoh* [1993] uses four sets of ADCP data from 1987 to 1989 obtained via shipboard measurements. Transport in the eastern channel is estimated to range between 0.59 and 1.3 Sv, with the typical current width ranging between 28 and 37 km. *Egawa et al.* [1993] use ADCP instruments mounted on ships of opportunity to measure currents in the strait. Results indicate that the seasonal transport variability is much less than previously obtained by hydrographic data.

In situ current meter measurements are limited due to the high regional fishing activity, which endangers conventional moorings that are deployed for more than just a few days [*Kawatate et al.*, 1988]. Many current meter moorings of the order of 1 day have been made in the strait. *Miita and Ogawa* [1984] estimate transport through the strait based on 431 in situ current meter stations, each of which sampled for at least 1 day, over the period 1920 to 1974. They estimate an average transport of 3.3 Sv through the southwestern entrance to the strait and 4.2 Sv northeast of Tsushima Island.

The development of trawl-resistant bottom mounts has allowed moorings to be deployed for long time periods. In this paper we examine data returned from 11 bottom-mounted ADCPs deployed in the strait from May 1999 through September 1999. The long-period moorings provide advantages over shipboard ADCP data. The transport estimates are much less affected by short time period events and the tides are more easily removed. One of the drawbacks to the bottom-mounted ADCPs is that the spatial data density is less than from shipboard ADCPs. Thus our goals in this paper are not only to estimate the transport from the bottom-mounted ADCPs but also to produce a reasonable estimate of the errors associated with the observed transport. In order to achieve this, careful attention is paid to the velocity covariance between different points in the strait.

The 11 ADCPs are deployed along two lines (Figure 1). The southern line covers the inflowing current, and the northern line covers the outflowing current. Each of these lines provides an independent transport estimate. Evaluation of our assumptions concerning covariances is tested by a comparison of the north and south line transports. For most times the transport estimates of the two lines are within one

Paper number 2000JC000289.

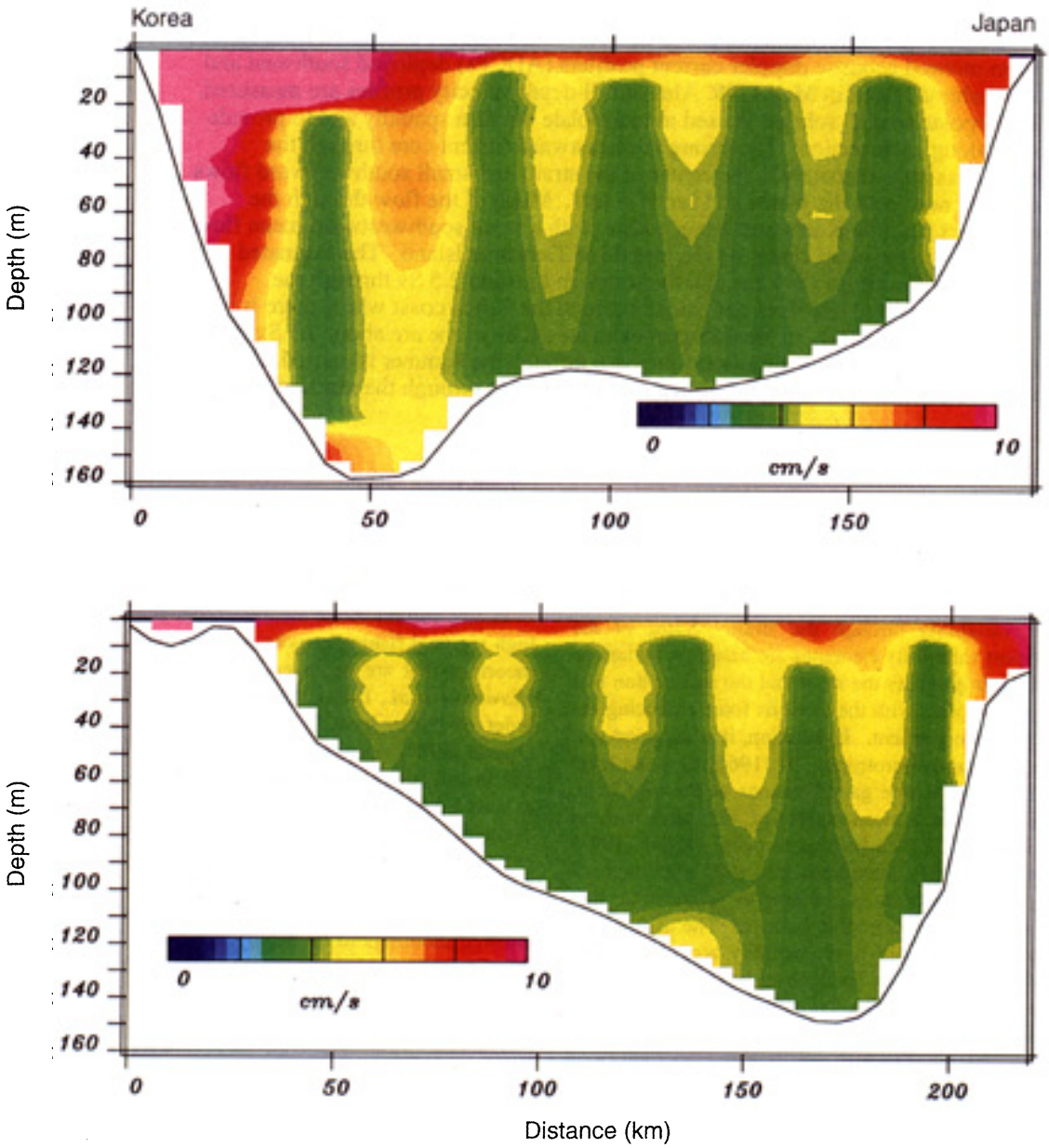

Plate 1. The estimated interpolation errors in the (top) northern mooring line and (bottom) southern mooring line show the minimal error at the mooring locations. The errors between mooring lines are generally small. This indicates that the instrument array is capable of resolving the typical spatial scales (Figure 2). Errors are larger near the surface and near the Korea coast along the northern line. These larger errors occur because the measurements do not extend to the surface, and the distance from the Korea coast to the first mooring is larger than the typical length scales.

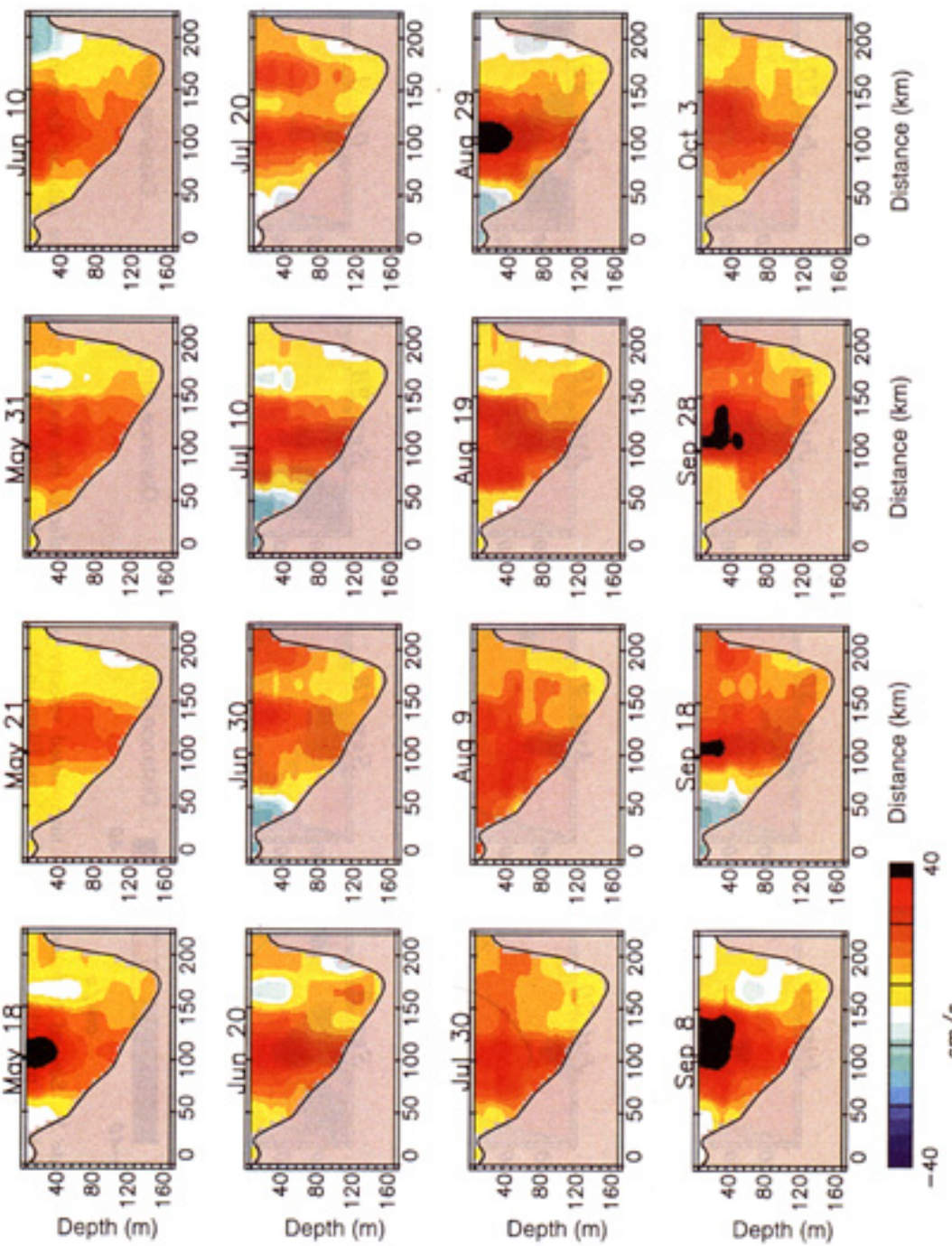

Plate 2. Several snapshots of the interpolated velocity perpendicular to the southern mooring line indicate the consistency of the central current core. Localized intense southward flowing currents appear sporadically near both the Japan and Korea coasts, at the surface, and in the subsurface.

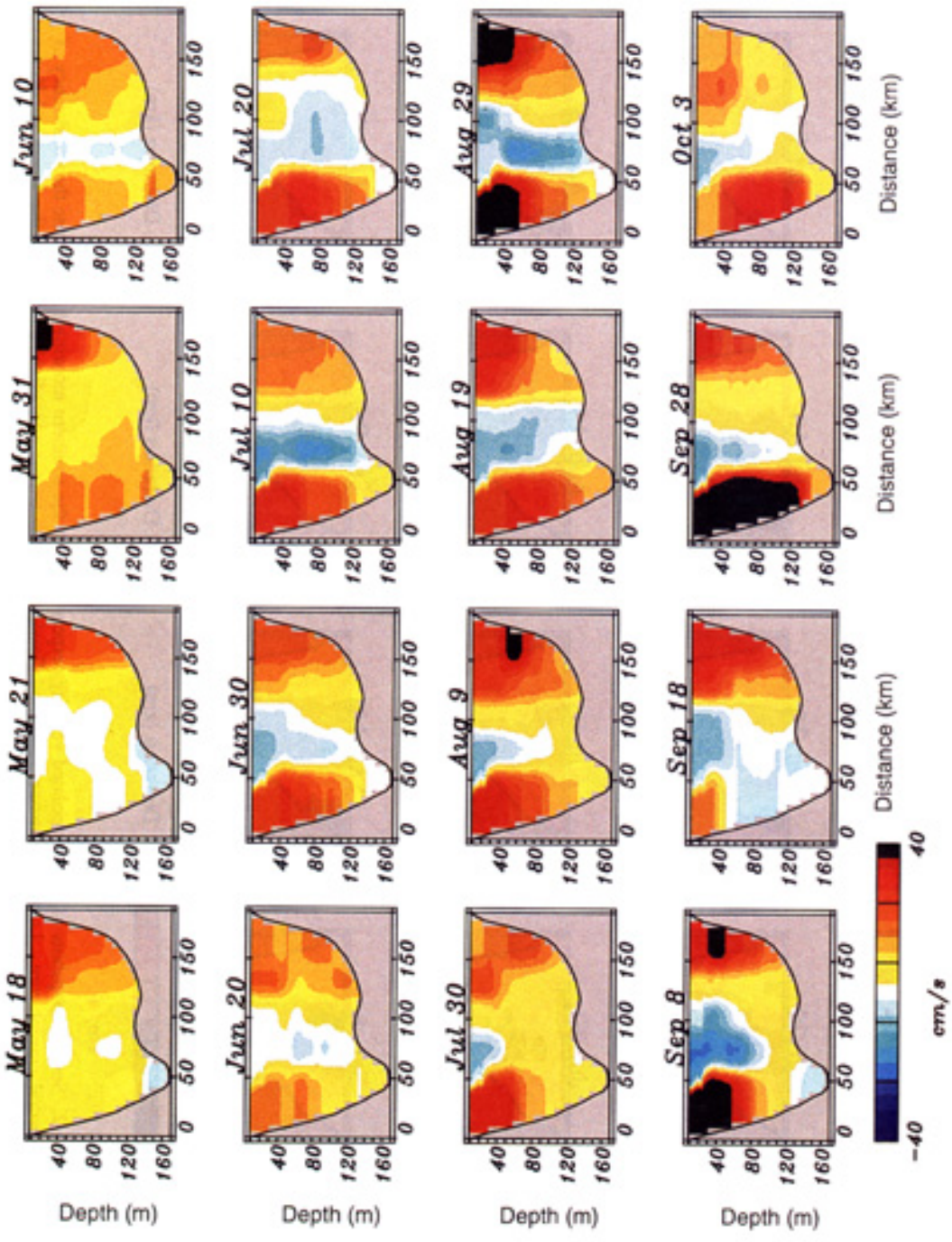

Plate 3. Several snapshots of the interpolated velocity perpendicular to the northern mooring line indicate the extreme variability, particularly northeast of Tsushima Island in the center of the section. The main northward flow occurs near the Korea and Japan coasts. The southwestward flowing current that creates the Korea Strait Bottom Cold Water is apparent in the deepest part of the trough and slightly toward the Korea coast.

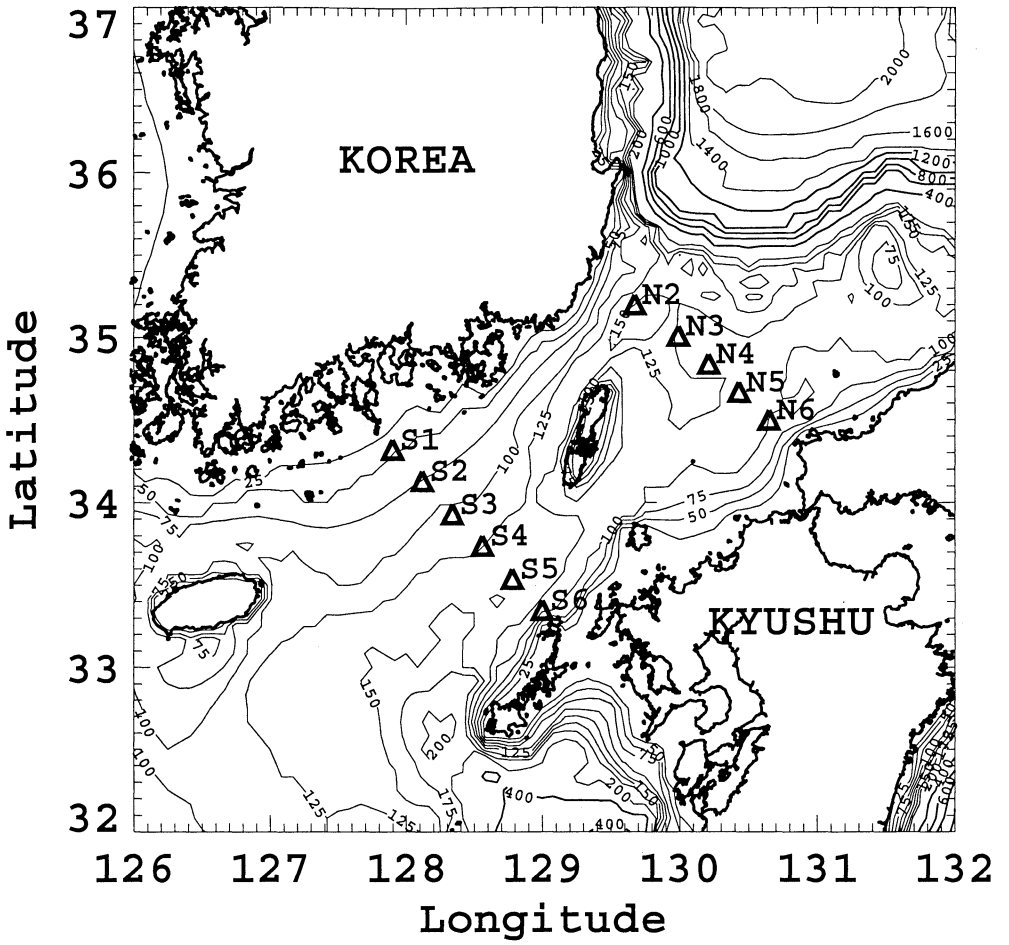

Figure 1. The acoustic doppler current profiler (ADCP) moorings are deployed along two lines, northeast (N2 through N6) and southwest (S1 through S6) of Tsushima Island, from May 1999 through September 1999.

standard deviation of the expected error estimates. However, there are several short time periods when the two transport estimates differ significantly. The implication is that our assumptions contained in the covariance structure are not correct during these times. The main sources of transport error are due to the inability of the bottom-mounted ADCPs to measure currents near the surface and the lack of data near the Korea coast along the north line.

First, we describe the instrumentation and deployment array in section 2. The formalism and development of the covariance functions used in the optimal interpolation scheme are discussed in section 3. The horizontal and vertical correlation scales are examined to provide an indication of the typical size of structures. Several interpolated snapshots, the time-varying total transport through the strait, and transport error estimates are then examined (section 4).

2. Instrumentation

Eleven current moorings are deployed along two lines, northeast and southwest of Tsushima Island, in the strait during May 1999 (Figure 1). The line southwest of Tsushima is referred to as the south line (S1 through S6) and the line northeast of Tsushima as the north line (N2 through N6). A trawl-resistant bottom mount is used for each mooring. It is a shallow dome-shaped enclosure that rests upon the bottom. The exposed side of the dome is relatively smooth in order to minimize snagging by fishing nets and lines. Instrumentation is enclosed safely within the dome about 0.5 m above the ocean bottom. Scraps of nets as well as evidence of trawl scrapings were found on the moorings at instrument retrieval. There is no evidence that these fishing activities adversely affected the data records. RD Instruments constructed the ADCP instruments. Profiles of u (eastward) and v (northward) components of velocity are recorded at 30-min intervals except at S5, N2, and N3, which are recorded at 15-min intervals. Depth resolution is 2 m at S1, S2, and N2 and 4 m for the other ADCPs. Data near the surface are contaminated by surface interference with the acoustic signal. The distance from the surface at which the interference occurs varies with instrument deployment depth. The ADCPs in the deep channels (at a depth of about 140 m) measure currents to within 20 m of the surface, while ADCPs in the shallower regions (100 m) measure to within 10 m of the surface. The measurements closest to the surface occur at mooring S2 (55 m depth), which measures to within 5 m of the surface.

Tidal variability within the strait is strong. Within this study we are concerned with the nontidal transport variations through the strait. Thus we remove the tidal variability to avoid contaminating covariance statistics and the results.

Eight tidal constituents (M2, S2, K1, O1, N2, P1, K2, and MU2) are removed by harmonic analysis from the time series of u and v velocities. This process is conducted for each velocity component at each depth bin independently. The barotropic and baroclinic tidal structures observed by the instruments are examined in detail by Teague *et al.* [2000]. There remain active tidal constituents, though the residual tidal variability is much smaller than the velocity variability. To be certain that the results for the covariance are not contaminated by tides, we filter the data with a Bartlett filter containing a first 0 power point at the 1 cycle per day frequency. The velocity measurements are interpolated in time to 12-hour intervals using a cubic spline for each time series of u and v so that all measurements at all locations occur at the same points in time. *Perkins et al.* [2000] also present a synopsis of the measurements.

3. Optimal Interpolation (OI)

An OI scheme [*Bretherton et al.*, 1976; *Lorenc*, 1981] is used to interpolate the ADCP observations horizontally and vertically along each mooring line. The solution along each mooring line is derived separately, and the velocities are interpolated at each time independent of other time points. In the OI the interpolated velocity component $\hat{u}$ is a linear combination of the observations:

$$\hat{u}(x,z,t) = \sum^{N} w_i m_i(t) , \qquad (1)$$

where N is the total number of u and v time series, w_i is the weight given to the i *th* measurement, and $m_i(t)$ is the i *th* measurement at time t. The i *th* measurement, $m_i(t)$, may be a measurement of either u or v. In this formulation the measurements of u and v are not treated separately. This allows the cross-covariance between the two velocity components to be included, and thus the results will not be sensitive to coordinate rotation.

By minimizing the expected error variance, the optimal solution for the measurement weights is given by the following linear equation:

$$\mathbf{Cw} = \mathbf{a} , \qquad (2)$$

where $\mathbf{C}$ is the covariance matrix of each variable with every other variable at the observation points, $\mathbf{w}$ is a column vector giving the weights in (1), and $\mathbf{a}$ is the column vector of the covariance between the interpolation variable at the interpolation point and the variables at the observation points. The OI is applied independently at each point in time, so the covariance matrix $\mathbf{C}$ contains only the covariance of one variable at one point in space to another variable at another point in space. The time-lagged covariance between points is not considered in this analysis. Since the time series of velocities at the moorings are relatively long, we use the time series of observations to calculate the covariance matrix $\mathbf{C}$. Thus we assume that the statistics are stationary and ergodic. The mean of each time series is removed prior to computing $\mathbf{C}$. The matrix $\mathbf{C}$ must be positive definite, and based on the observations the covariance matrix is only positive semidefinite. An eigen-decomposition of $\mathbf{C}$ indicates that the last 100 of 324 eigenvalues are more than 8 orders of magnitude smaller than the first eigenvalue. In order to make the matrix inversion stable, a slight amount of white noise (3 cm/s RMS) is added to the diagonal elements of the covariance matrix.

The typical horizontal and vertical length scales are computed to provide a simple examination of correlation scales. To compute the horizontal length scales, the correlations of a velocity time series at a particular depth bin with the velocity time series of the neighboring moorings at the same depth are calculated. If the neighboring moorings do not contain a bin at the same depth, the closest depth bin is chosen. From the correlation coefficient the horizontal length scale is determined assuming that the horizontal-distance-lagged correlation function is Gaussian:

$$r = e^{-x^2/l^2} , \qquad (3)$$

where r is the average correlation to neighboring moorings, x is the distance between the two moorings, and l is the horizontal length scale. Of course, the assumption of the covariance form used in (3) is arbitrary, and we choose the Gaussian form because of the relatively simple structure as well as the lack of a more appropriate choice. The horizontal length scales at each mooring site are presented in Figure 2. Generally, the length scales are between 15 and 30 km. The Rossby radius of deformation is 18 km [*Cho and Kim*, 1998], and the width of the current cores observed by ship ADCP is between 28 and 37 km [*Katoh*, 1993]. Thus the horizontal length scales obtained here are in agreement with theoretical and previously observed scales. Since the average spacing between moorings is 25 km, the ADCP moorings are only marginally capable of resolving typical horizontal scales. The scales computed here are assumed to be stationary in time. Features with spatial scales smaller than the instrument spacing occur, and these features are not resolved. The one area where the moorings are not capable of sampling the typically observed horizontal length scales is located along the north line near the Korea coast. For this reason the subsequent OI interpolation error fields indicate a larger interpolation error at this location.

The horizontal length scales indicate a local minimum at a depth of about 30 m in all the southern moorings and most of the northern moorings. This is the typical depth of the thermocline during this time of year. Because of the strong vertical density stratification, currents would be expected to behave as a two-layer baroclinic system. Thus correlations of currents with each other above the thermocline and correlations of currents with each other below the thermocline would be higher than correlations of currents across the thermocline.

The vertical scales are computed in a similar manner. At a given mooring, for a particular depth, the correlation of the velocity time series to the time series at neighboring depth bins is computed. Again, using the assumption that the lagged correlation function in the vertical is Gaussian, the depth scale is computed from the observed correlation value (Figure 3). The vertical length scales are roughly 20 m near the bottom and decrease toward the surface. Wind forcing creates a strong vertical shear and turbulence near the surface, and thus the vertical correlation distance is smaller near the surface.

The next step in the OI is to specify the $\mathbf{a}$ vector of the covariance between the interpolation variable at the interpolation point and the variables at the observation points. We use the observed covariances within the matrix $\mathbf{C}$

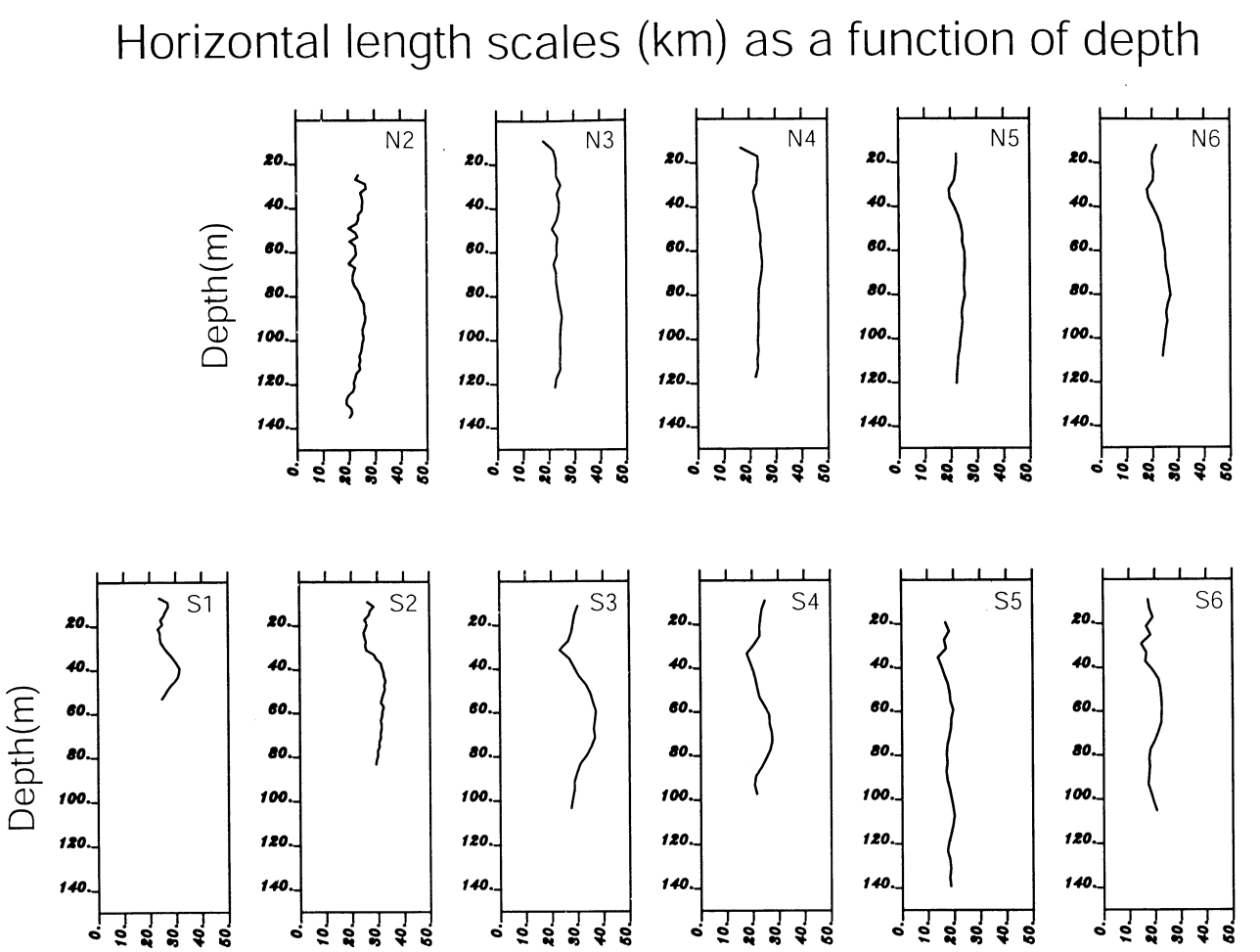

Figure 2. Horizontal length scales (km) are based on the correlation of the velocity time series with the velocity time series at neighboring moorings and the assumption that the horizontal-distance-lagged correlation function is Gaussian. The length scales are computed separately for each depth bin of each mooring.

to determine the covariances within the vector $\mathbf{a}$. First, the covariance matrix $\mathbf{C}$ may be represented as

$$\mathbf{C} = [\mathbf{c}_1, \mathbf{c}_2, \cdots, \mathbf{c}_N], \tag{4}$$

where $\mathbf{c}_j$ is the $j\,th$ column vector. The covariance between the $j\,th$ observation variable and all other observation variables is $\mathbf{c}_j$. For an interpolation point at the same position as the $j\,th$ measurement point, $\mathbf{c}_j$ should be used as $\mathbf{a}$. As the interpolation point moves from the observation point, the covariances in $\mathbf{a}$ should decrease. To represent this decrease, the horizontal length scales $\mathbf{c}_j$ derived above are used. In addition, if the interpolation point is between two mooring sites, the covariance from each mooring should influence the value of $\mathbf{a}$. Thus the value of $\mathbf{a}$ is determined from

$$\mathbf{a} = \mathbf{c}_k \frac{x_m - x}{x_m - x_k} e^{-(x_k - x)^2 / l_k^2} + \mathbf{c}_m \frac{x_k - x}{x_k - x_m} e^{-(x_m - x)^2 / l_m^2}, \tag{5}$$

where $\mathbf{c}_k$ is the observed covariance at position x_k, $\mathbf{c}_m$ is the observed covariance at position x_m, l_k is the length scale at the closest depth bin from mooring k, and l_m is the length scale at the closest depth bin from mooring m. The two quantities $(x_m - x)/(x_m - x_k)$ and $(x_k - x)/(x_k - x_m)$ represent the fraction of distance of the interpolation point x from each of the mooring positions x_m and x_k. Thus if $x = x_k$ the value of $\mathbf{a}$ is taken as $\mathbf{c}_k$, and if $x = x_m$ the value of $\mathbf{a}$ is taken as $\mathbf{c}_m$. This formation sets $\mathbf{a}$ to the observed covariance when the interpolation point is at the observation points, and sets $\mathbf{a}$ to a linear-weighted combination of the observed covariance when interpolating between observation points. When extrapolating beyond the end mooring of the mooring lines, only one $\mathbf{c}_k$ is available for use. Note that the $\mathbf{C}$ matrix is based on observed covariances, and the Gaussian length scales are not used. The $\mathbf{a}$ vector is a linear combination of the columns of $\mathbf{C}$, and the linear coefficients depend on the Gaussian length scales.

The OI scheme assumes that the measurements have 0 mean. All the covariances computed above are based on the observation time series with means removed. However, the transport through the strait at any given time is not 0. Thus once $\mathbf{a}$ is determined and the measurement weights are calculated from (2), the weights are modified to provide a sum of 1, and the measurements without the mean removed are used in (1) to yield an unbiased result. Our choice for $\mathbf{a}$ from equation (5) and the scaling of the weights to 1 cause the OI to generate a linear interpolation between the mooring positions and an extrapolation of the observations beyond the end of the mooring line to the shoreline.

Even though the OI scheme is suboptimal (we have changed the weights from the optimal values) and provides only a linear interpolation, the scheme still allows for an

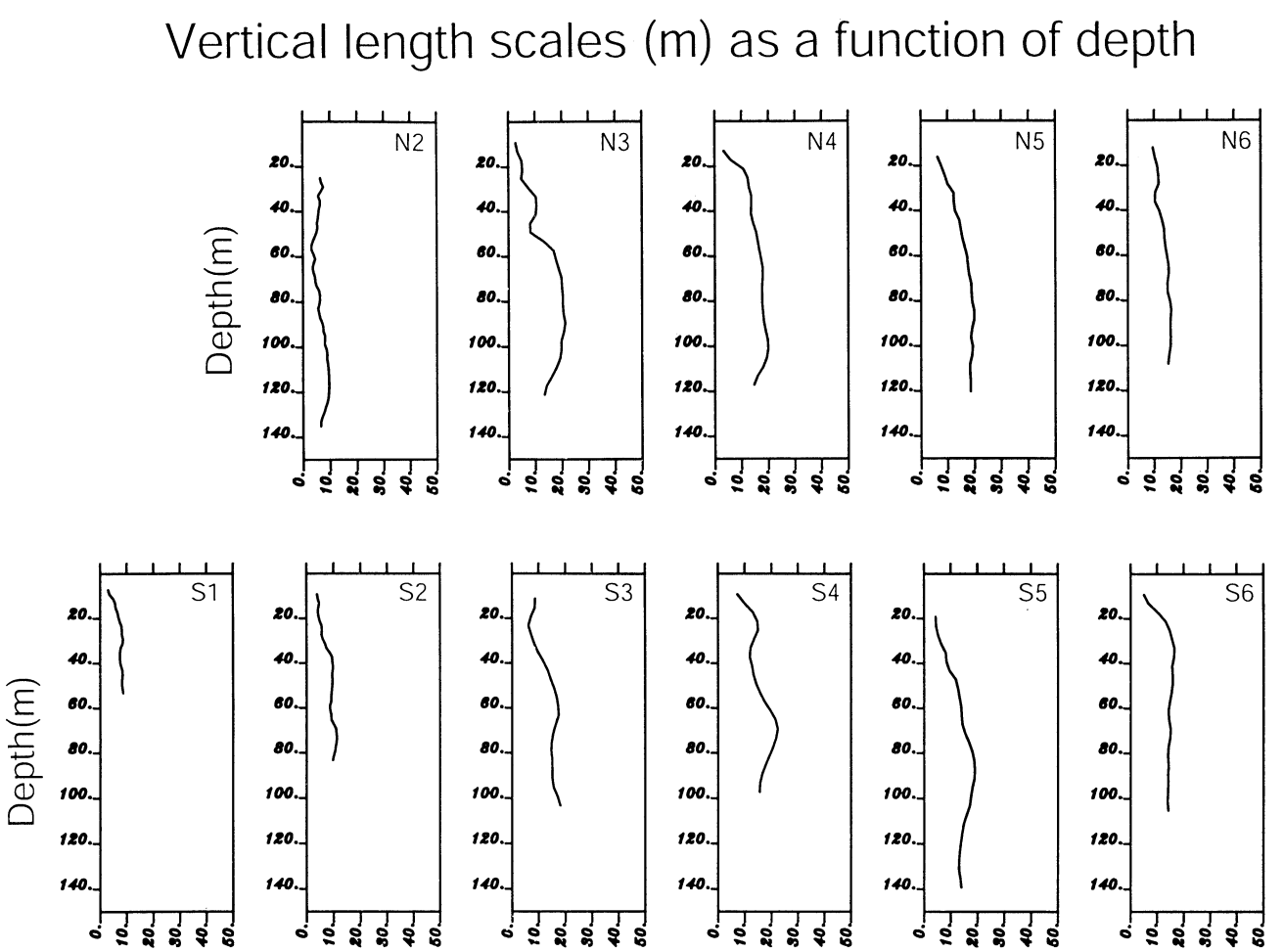

Figure 3. Vertical length scales (m) are based on the correlation of the velocity time series with the velocity time series at neighboring vertical bins and the assumption that the vertical-distance-lagged correlation function is Gaussian. The length scales are computed separately for each depth bin of each mooring. The vertical length scales generally indicate a decreased length near the surface, as would be expected due to wind influence.

error estimate of the interpolated values. The error estimate is computed by

$$V = v - 2\sum_{i}^{N} w_i a_i + \sum_{i}^{N}\sum_{n}^{N} w_i w_n c_{in}, \qquad (6)$$

where v is the expected variance at the interpolation point. Equation (6) provides the expected interpolation error for any set of chosen weights. However, because we have changed the weights w_i to avoid biasing the data with a nonzero mean, the solution no longer provides the minimum error variance, but instead provides the minimum bias.

Examples of the interpolated velocity error estimates across the north and south sections are presented in Plate 1. The error estimates are constant for all times as the values of the observation covariance matrix **C** and the interpolation covariance vector **a** are time invariant. As expected, the interpolation errors are minimum at the observation points. The mooring positions are apparent as lines of minimum error extending from the bottom to within about 15 m of the surface. Interpolation errors are generally larger near the surface due to the lack of measurements. In addition, along the north mooring line, interpolation errors are larger near the Korea coast since no measurements are within the observed horizontal length scales (Figure 2).

4. Transport Variations

Representative snapshots of the velocity perpendicular to each line provided by the OI are shown in Plates 2 and 3. The u and v velocity components are interpolated separately, and the velocity perpendicular to the mooring lines is calculated as

$$v_p = u\,nx + v\,ny,$$

where nx and ny are the components of the unit vector normal to each mooring line. The velocity snapshots for the southern mooring line (Plate 2) indicate a current core generally within the central portion of the strait. Sporadic southwestward flows of moderate intensities appear mainly near the Korea and Japan coasts.

The velocities across the northern mooring line (Plate 3) indicate more variability than the velocities across the southern mooring line. The largest variability occurs in the central portion of the strait, which is in the lee of Tsushima Island. Strong southwestward flow events occur in the central portion of the strait. *Katoh* [1993] and *Isobe et al.* [1994] have also observed these events through ship ADCP measurements. These events could lead to the southward flow along the eastern side of Tsushima Island as observed in

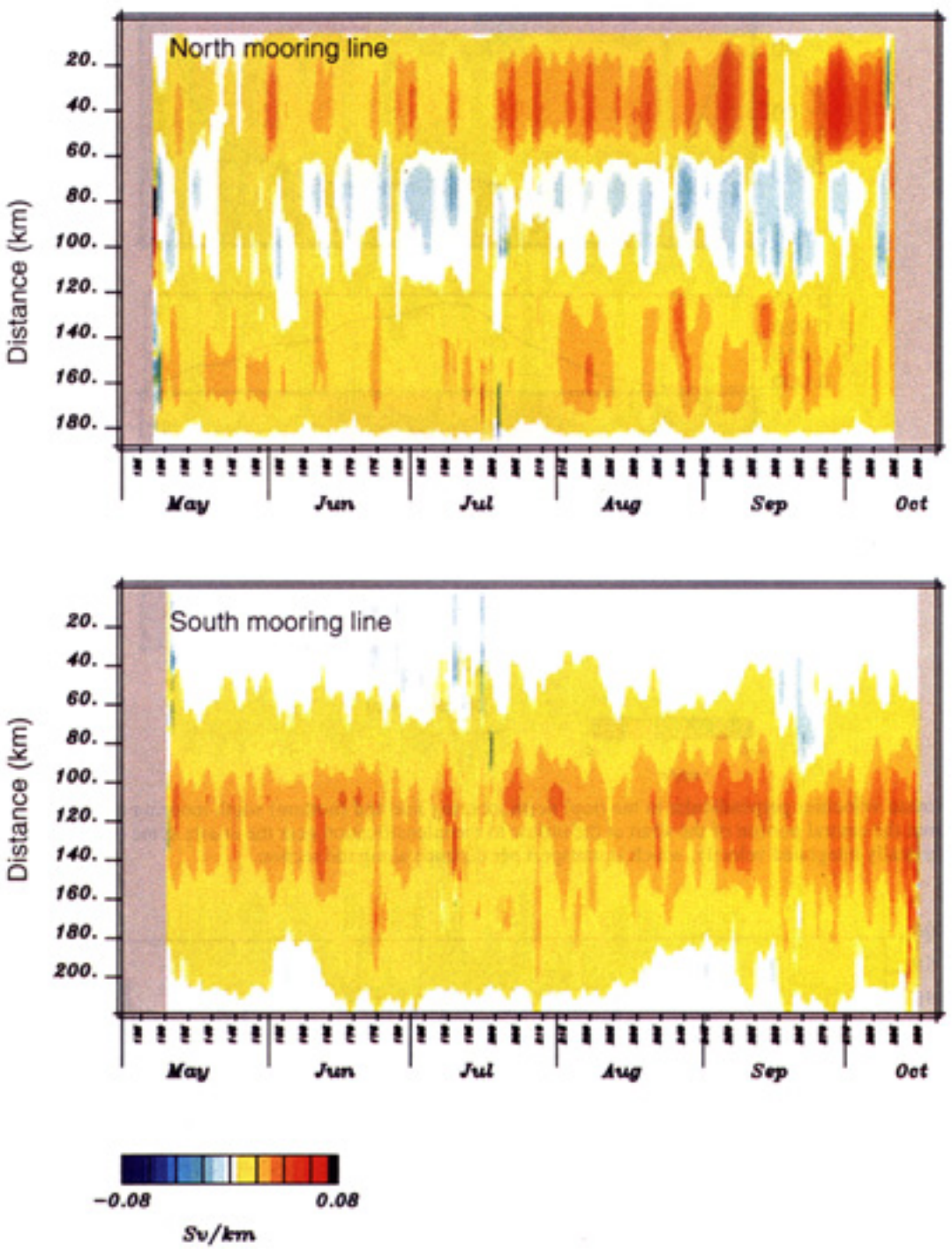

Plate 4. The vertically integrated velocity as a function of distance from Korea and time indicates short-period variations as well as the sporadic flow reversals in the lee of Tsushima Island. The general increasing transport through the summer occurs in the center of the southern line and toward the Korea coast in the northern line.

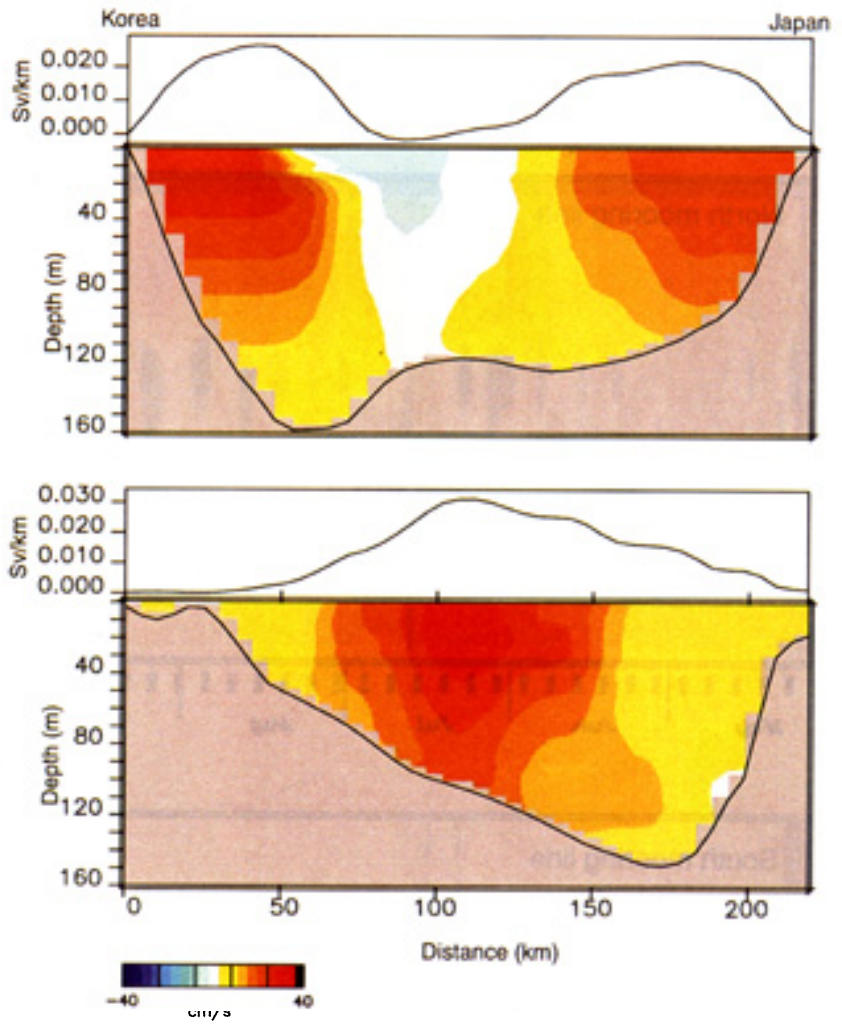

Plate 5. The mean velocities perpendicular to the (top) north mooring line and (bottom) south mooring line indicate the change in transport from the central portion of the strait at the inflow to the intensification near the coasts at the outflow. The line plots indicate the vertically integrated velocity, which is transport per distance along the section.

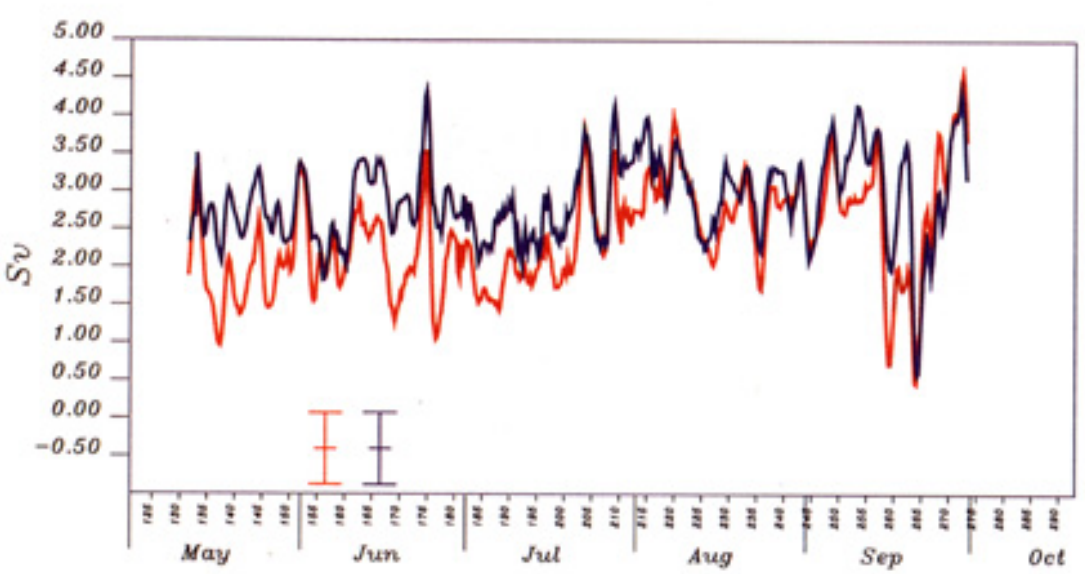

Plate 6. The transports estimated from the southern mooring line (blue) and the northern mooring line (red) indicate a time-averaged mean of 2.9 Sv and 2.5 Sv, respectively. The RMS transport error estimate at any single time is shown in the lower left by the confidence intervals. These error estimates are time invariant.

the historical data of *Miita and Ogawa* [1984] and *Egawa et al.* [1993]. The northeastward flows along the Korea and Japan coasts are also strongly variable, and intense currents occur off both coasts at different times. Generally, the currents intensify toward the coast, as has been observed in the historical data sets [*Miita and Ogawa*, 1984; *Egawa et al.*, 1993]. An occasional southwestward flow appears in the deepest portion of the trough along the northern section. *Cho and Kim* [1998] observe the effects of this southwestward flow through changes in temperature and salinity within the trough. This flow brings cold saline water into the strait and forms the Korea Strait Bottom Cold Water (KSBCW). *Cho and Kim* [1998] observe the largest KSBCW water mass extent during August.

The velocity is integrated over depth to produce the time variability of the transport along each mooring line (Plate 4), and the velocity snapshots constructed from the 12-hourly data are averaged over time to estimate the average transport perpendicular to each mooring line (Plate 5). The average transport is northward except at the surface in the lee of Tsushima Island (Plate 5). The time variability of vertically integrated flow across the northern mooring line (Plate 4) indicates this area at about 80 km along the mooring line as containing short-period southwestward flow events. The historical interpretation of *Suda and Hidaka* [1932] and *Uda* [1934] that the Tsushima Warm Current (TWC) splits into three distinct branches upon entering the Sea of Japan is still widely accepted, although others have regarded the TWC as a single meandering current that episodically sheds eddies. In contemporary literature the three branches correspond to the Nearshore Branch, the Offshore Branch, and the East Korean Warm Current from east to west, respectively.

The nature of the branching is very complex and quite variable in space and time. For instance, concurrent sea surface temperature (SST) images and hydrographic data [*Kim and Legeckis*, 1986] demonstrate that during 1981-1982 the East Korean Warm Current (EKWC) and Nearshore Branch exhibit independent pathways. The complex structure of these currents is also described via ADCP data and concurrent hydrographic data [*Katoh*, 1994]. Those results usually show the bifurcation of the TWC south of 37°N into the Offshore Branch and EKWC during 1976-1990, but notable exceptions are 1976, 1982, and 1990 when only northward flow (the EKCW) is recognized, and 1981 and 1986 when only eastward flow (the Nearshore Branch) is recognized.

In this study the branching of the TWC into the EKWC and Nearshore Branch is apparent as the single current core across the southern mooring line splits into two cores across the northern mooring line with the cores concentrated along the Korea and Japan coasts (Plate 4 and Plate 5). The Offshore Branch is not present in the mean velocity across the northern mooring line. There is actually a southwestward flow through the central area of the mooring line. If the Offshore Branch is present during this time, it must branch from either the Nearshore Branch or the East Korean Warm Current further downstream.

The time-varying transport across each mooring line is computed from the velocities at the 12-hour intervals. The total transport across each line is the integral over the cross-sectional area of the velocity normal to the section:

$$T = \iint_{x,z} u\,nx + v\,ny\,dx\,dz\,, \tag{7}$$

Each mooring section produces an independent estimate of the total transport. An important question concerns whether the transport estimates agree within expected measurement errors. This question is addressed by computing the expected error in the total transport. If the errors associated with the interpolation at two different spatial points were assumed independent at a particular time, the error in the transport estimate would be unreasonably small. Since the interpolated velocity estimates at two neighboring points are strongly correlated, errors in the interpolated velocities are strongly correlated. To demonstrate, let the velocity error at a particular time be denoted by

$$u_e(x,z) = u(x,z) - u_T(x,z)\,, \tag{8}$$

where $u_T(x,z)$ is the true velocity. Then ignoring the cross error between velocity components, the expected transport error variance is given by

$$\begin{aligned}
\sigma_T^2 &= \left\langle \begin{matrix} \iint_{x,z} u_e(x,z)nx + v_e(x,z)ny\,dx\,dz, \\ \iint_{x,z} u_e(x',z')nx + v_e(x',z')ny\,dx'\,dz' \end{matrix} \right\rangle \\
&= \left\langle \iint_{x',z'} \iint_{x,z} \begin{matrix} \left(u_e(x,z)nx + v_e(x,z)ny\right)\times \\ \left(u_e(x',z')nx + v_e(x',z')ny\right)dx\,dz\,dx'\,dz' \end{matrix} \right\rangle \\
&= \iint_{x',z'} \iint_{x,z} \left(\begin{matrix} \left\langle u_e(x,z)u_e(x',z')\right\rangle nx^2 + \\ \left\langle v_e(x,z)v_e(x',z')\right\rangle ny^2 \end{matrix} \right) dx\,dz\,dx'\,dz'\,.
\end{aligned} \tag{9}$$

The angle brackets indicate an expected value. To calculate the expected transport error variance, we must specify the spatial error covariance of the interpolated velocity. The interpolation error estimates previously discussed (Plates 1 and 2) indicate the interpolation error only at a single point and do not indicate how the error at one point is related to the error at another point. We specify the spatial relation between interpolation errors by using the horizontal and depth length scales previously determined (Figures 2 and 3):

$$\begin{aligned}
\left\langle u_e(x,z)u_e(x',z')\right\rangle &= V_u e^{-(x-x')^2/l_x^2} e^{-(z-z')^2/l_z^2}\,, \\
\left\langle v_e(x,z)v_e(x',z')\right\rangle &= V_v e^{-(x-x')^2/l_x^2} e^{-(z-z')^2/l_z^2}\,,
\end{aligned} \tag{10}$$

where V_u and V_v are the interpolation variances for the u and v velocity fields determined by equation (6), and l_x and l_z are the horizontal length and vertical length scales. The standard deviation intervals determined by equation (10) are plotted along with the transport estimates (Plate 6). The time-averaged transports are 2.9 Sv across the southern mooring line and 2.5 Sv across the northern line. At any particular time the error estimate is about 0.5 Sv RMS. The transports estimated from the north and south mooring lines are generally within one standard deviation. During May and June the north transport estimate is consistently lower than the south transport estimate. There are also individual times when the transports differ significantly, for example, around day 260. This time occurs in September during a large wind event as indicated by the wind stress magnitude at 34°N, 128°E from the Navy Operational Global Atmospheric Prediction System (NOGAPS) (Figure 4).

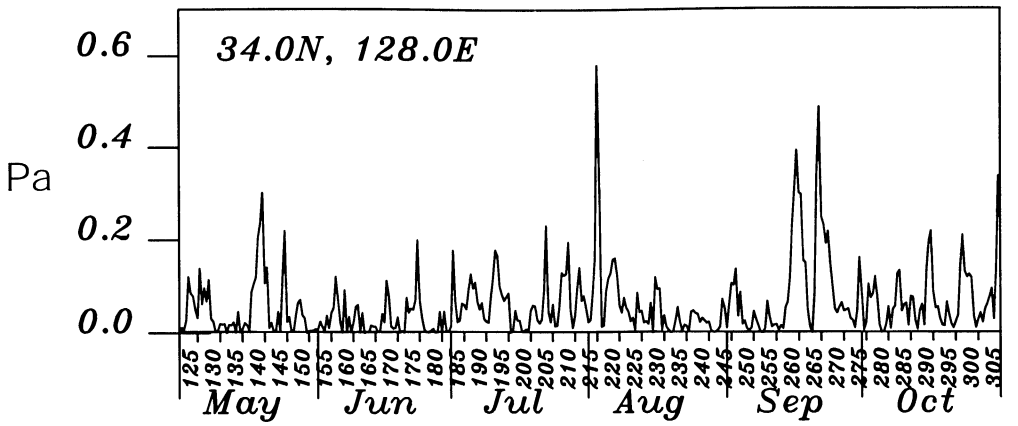

Figure 4. Wind stress magnitude within the Korea Strait as modeled by the Navy Operation Global Atmospheric Prediction System (NOGAPS) indicates a strong typhoon event in the middle of September 1999.

There is also a general increasing transport trend in both time series of Plate 6. From the vertically integrated velocity (Plate 4) it appears that the increasing transport occurs in the center of the southern mooring line and in the northern portion of the north mooring line. The seasonal transport variability has been observed to be increasing through summer and decreasing during winter. The results here indicate that the increasing summer transport is carried mostly in the flow along the Korea side of the strait, which would lead into the East Korean Warm Current.

The discrepancy between the two transport estimates indicates that our assumptions in the covariance structure are not correct during these times. The covariance structure is based on an average of statistics over the entire deployment time (which is why our interpolation and transport error estimates are time invariant). During certain times the synoptic currents and their relations are significantly different from those typically observed.

Since the northern mooring line transport is 0.4 Sv smaller than that of the southern line, it likely does not contain sufficient sampling to completely resolve the spatial structure. Several processes may lead to transport not observed by the northern line. The typical scales observed are between 15 and 30 km. However, this does not imply that shorter spatial scales sometimes exist. That is, narrow currents could form between the mooring sites. High-resolution snapshots of currents across the strait obtained by ship-mounted ADCP [*Isobe et al.*, 1994] indicate currents more narrow than the mooring spacing do occur.

A second possible process that the northern mooring line may not resolve is a narrow current along the Korea coast. The interpolation error along the northern mooring line indicates relatively large errors near the Korea coast (Plate 2). The Korea coast is typically an area of large observed currents. From historical current meter data [*Miita and Ogawa*, 1984; *Egawa et al.*, 1993], the velocity decreases with distance from the Korea coast. The velocity intensification near the coast is implied in the baroclinically induced transport [*Isobe*, 1994] and is more dramatically apparent in snapshots measured by ship-mounted ADCP [*Katoh*, 1993; *Isobe et al.*, 1994]. The interpolation scheme here simply extrapolates the velocity value at the mooring to the coast. Thus the northern mooring line would underestimate transport due to an intensified coastal current.

Finally, it is possible that the velocity field becomes surface intensified. The bottom-mounted ADCP instrument measurements do not measure the near-surface layer. This is apparent in the interpolation error fields as the expected error increases near the surface. The water properties from the East China Sea develop warm and relatively fresh water due to high summer heat flux and large river outflow from the Yellow Sea. This water is much less dense than the Japan Sea Proper water or the Salinity Minimum Layer water [*Cho and Kim*, 1998]. The less dense northward flowing East China Sea water has a tendency to override the denser water at the bottom of the north end of the strait. This would lead to a surface intensification that could explain the smaller transport observed along the northern mooring line.

5. Conclusions

Transport estimates in the Korea-Tsushima Strait are made using measurements from two lines of bottom-mounted ADCP instruments deployed from May 1999 through September 1999. The time-averaged transports are 2.9 Sv through the southern line and 2.5 Sv through the northern line. Transport estimate errors based on the horizontal and depth length scales observed by the instruments are about 0.5 Sv. The majority of transport through the south mooring line is centered within the strait. Along the north mooring line the transport is concentrated toward the Korea and Japan coasts with a small southwestward transport northeast of Tsushima Island. The increasing summer transport is carried within the center of the strait along the southern line and toward the Korea side of the strait along the northern line. The transport estimates between the two lines are within one standard deviation throughout most of the observation period, though significant differences occur at several times. Possible reasons for the difference between the north and south transport estimates are currents much more narrow than those usually observed, intensification of the currents near the Korean coast along the northern line, and surface intensification as the less dense East China Sea water overrides the more dense water at the exit of the strait.

Acknowledgments. We thank two anonymous reviewers for taking their time to help improve this manuscript. This work was sponsored by the Office of Naval Research (program element PE0601153N) as

part of the projects "Yellow and East China Seas Response to Winds and Currents", and "Dynamical Linkage of the Asian Marginal Seas". This work is contribution JA/7323-98-0068 of the Naval Research Laboratory.

References

Bretherton, F. P., R. E. Davis, and C. B. Fandry, A technique for objective analysis and design of oceanographic experiments applied to MODE-73, *Deep Sea Res., 23*, 559-582, 1976.

Cho, Y. K., and K. Kim, Structure of the Korea Strait Bottom Cold Water and its seasonal variation in 1991, *Cont. Shelf Res., 18*, 791-804, 1998.

Egawa, T., T. Nagata, and S. Sato, Seasonal variation of the current in the Tsushima Strait deduced from ADCP data of ship-of-opportunity, *J. Oceanogr., 49*, 39-50, 1993.

Isobe, A., Seasonal variability of the barotropic and baroclinic motion in the Tsushima-Korea Strait, *J. Oceanogr., 50*, 223-238, 1994.

Isobe, A., S. Tawara, A. Kaneko, and M. Kawano, Seasonal variability in the Tsushima Warm Current, Tsushima-Korea Strait, *Cont. Shelf Res., 14*, 23-35, 1994.

Katoh, O., Detailed current structures in the eastern channel of the Tsushima Strait in summer, *J. Oceanogr., 49*, 17-30, 1993.

Katoh, O., Structure of the Tsushima Current in the southwestern Japan Sea, *J. Oceanogr., 50,* 317-338, 1994.

Kawatate, K., T. Miita, Y. Ouchi, and S. Mizuno, A report on failures of current meter moorings set east of Tsushima Island from 1983 to 1987, *Prog. Oceanogr., 21*, 319-327, 1988.

Kim, K., and R. Legeckis, Branching of the Tsushima Current in 1981-83, *Prog. Oceanogr., 17*, 265-276, 1986.

Lorenc, A. C., A global three-dimensional multivariate statistical interpolation scheme, *Mon. Weather Rev., 109*, 701-721, 1981.

Miita, T., and Y. Ogawa, Tsushima currents measured with current meters and drifters, in *Ocean Hydrodynamics of the Japan and East China Seas*, edited by T. Ichiye, *Elsevier Oceanog. Ser.*, vol. 39, pp. 67-76, Elsevier Sci., New York, 1984.

Perkins, H. T., W. J. Teague, G. A. Jacobs, K. I. Chang, and M. S. Suk, Currents in Korea-Tsushima Strait during summer 1999, *Geophys. Res. Let., 27,* 3033-3036, 2000.

Suda, K., and K. Hidaka, The results of the oceanographical observations aboard R.M.S. *Syunpu Maru* in the southern part of the Sea of Japan in the summer of 1929 (in Japanese), 1, *J. Oceanogr. Imp. Mar. Observ., 3*, 291-375, 1932.

Teague, W. J., H. T. Perkins, G. A. Jacobs, and J. W. Book, Tide observations in the Korea-Tsushima Strait, *Cont. Shelf Res.*, in press, 2000.

Uda, M., The results of simultaneous oceanographical investigations in the Japan Sea and its adjacent waters in May and June, 1932 (in Japanese), *J. Imp. Fish. Exp. Stn., 5*, 57-190, 1934.

Yi, S. U., Seasonal and secular variations of the water volume transport across the Korea Strait, *J. Oceanogr. Soc. Korea, 12*, 7-13, 1966.

P. J. Hogan, G. A. Jacobs, H. T. Perkins, and W. J. Teague, Naval Research Laboratory, Code 7323, Stennis Space Center, MS 39529. (jacobs@nrlssc.navy.mil)

(Received February 16, 2000; revised October 16, 2000; accepted November 6, 2000.)